

Lasers in Manufacturing Conference 2017

## Selective laser melting of NiTi powder

A. Domashenkov<sup>a,\*</sup>, M. Doubenskaia<sup>a</sup>, I. Smurov<sup>a</sup>, M. Smirnov<sup>b</sup>, A. Travianov<sup>b</sup>

<sup>a</sup>Lyon University, ENISE, LTDS Laboratory, UMR CNRS 5513, 58 rue Jean Parot, 42023 Saint-Étienne Cedex 2, France

<sup>b</sup>Nation University of Science & Technology (MISIS), 4 Leninsky pr., 119049, Moscow, Russia

---

### Abstract

Selective laser melting (SLM) is applied to develop samples from NiTi powder using preheating up to 600°C (to reduce thermal gradients) and different substrate materials: 304L, Ti-6Al-4V, Inconel 718. It is found that the composition of substrate influences the resulting porosity and eventual cracking of NiTi layers. The principle phase of the obtained samples is NiTi B2 austenite. Some minor picks of R martensite are detected, as well as the formation of Ni<sub>4</sub>Ti<sub>3</sub> precipitates. The microstructure of the samples is austenitic with martensite-like zones of the R phase. Martensitic structure is found inside the cracks. Mechanical properties are measured by nanoindentation: Young's modulus of B2 austenite is 108 GPa and the hardness is equal to 8.1 GPa; for R martensite Young's modulus is 84.1 GPa and the hardness is equal to 5.7 GPa.

Keywords: selective laser melting, intermetallics; Nitinol, nanoindentation, mechanical properties.

---

### 1. Introduction

NiTi, also known as Nitinol, is an intermetallic alloy of nickel and titanium, in which the two elements are present in approximately equal atomic percentages. Shape memory effect (SME) and superelasticity (SE) are related to the reversible nature of the martensitic transformation that appears in NiTi. The shape memory effect is the ability to recover the original form after deformation by heating above the transformation temperature. NiTi transforms from the austenite B2 phase to the monoclinic martensite B19' phase with an intermediate orthorhombic R phase from which the SME and the SE result. Superelasticity takes place in a narrow temperature range above the transformation temperature, in this case the elasticity of NiTi can exceed the initial value up to 30 times (Yoneyama & Miyazaki, 2008, Sauthoff, 2008).

---

\* Corresponding author. Tel.: + 33 7 82 03 04 14; fax: + 33 4 77 74 34 97.  
E-mail address: Alexey.domashenkov@enise.fr; a.domashenkov@gmail.com.

Additive manufacturing (AM) of functional objects is an emerging fabrication concept allowing development of novel functional products as well as customized and unique parts. Among AM technologies, selective laser melting (SLM) is one of the promising methods to manufacture complex functional components for various industrial applications. SLM is a layer-wise process, where a 3D CAD model is sliced into a finite number of layers (cross-sections) by special software. Further, during the building of a 3D physical object in an SLM machine, a layer of powder corresponds to each cross-section. A powder bed is fused by laser passes so that it provides metallurgical bonding with the previously deposited layer. The desired 3D model is manufactured layer-by-layer as a superposition of the cross-sections.

## 2. Material and methods

The Nitinol powder was purchased from LPW Technology Ltd. The chemical composition according to manufacturer specification is shown in Table 1.

Table 1. Chemical composition of NiTi powder

Elem.	C	Co	Cr	Cu	Fe	H	N	Nb	Ni	O	Ti
Wt.%	0.04	<0.01	<0.01	<0.01	<0.1	0.001	0.01	<0.005	57.0	0.08	Bal.

The particles have generally a spherical form, according to SEM analysis (Fig. 1). The powder size distribution (Fig. 2) was studied using a granulomorphometer ALPAGA 500NANO (OCCHIO S.A.).

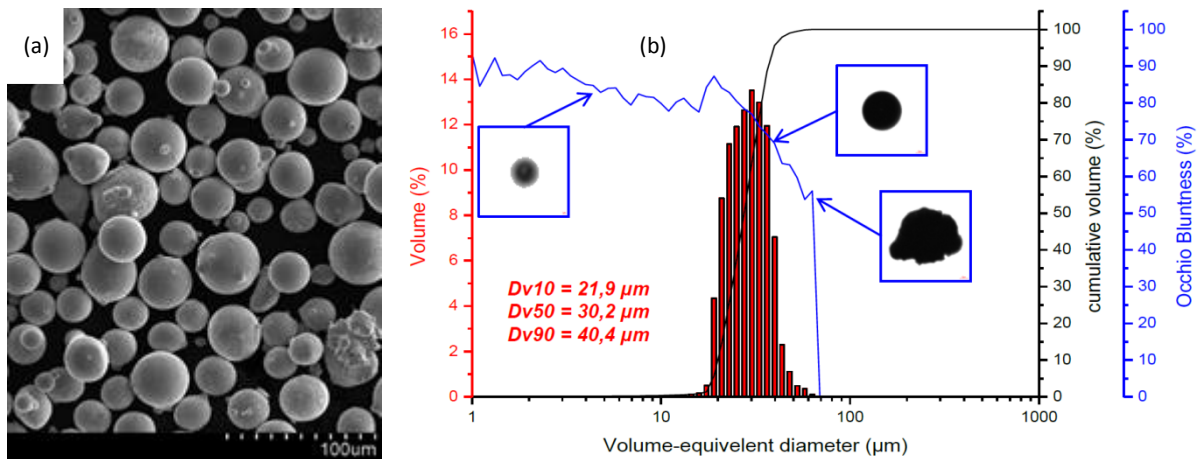


Fig. 1. (a) SEM image of NiTi powder (b) NiTi powder size distribution

SLM process was carried out using Phenix Systems «PM-100» machine equipped with a CW fiber laser of 1073 nm wavelength (IPG Photonics Corp.), 200 W maximum power and a spot diameter of 70 μm.

Steel 304L, Ti-6Al-4V and Inconel 718 were used as substrate materials. The building chamber is protected by argon (<1000 ppm of oxygen).

Scanning Electron Microscopy (SEM) images of the powder and samples are obtained by an electron microscope S-3400N (Hitachi High-Technologies Corporation), equipped with a NORAN energy-dispersive X-

ray spectrometer.

The samples for metallographic analysis are prepared using Phoenix 4000 (BUEHLER, USA) grinder polisher. Optical micrography is performed with ZEISS Axioscope A1 optical microscope. X-ray diffraction (XRD) measurements for the samples are obtained on DRON-4 automatic diffractometer using monochromatic  $\text{CuK}\alpha$  radiation in step-by-step scanning mode in the  $2\theta$  range of  $10\text{-}110^\circ$  with the scan increment of  $0.1^\circ$

The microhardness tests are performed with BUEHLER Micromet 5104, using a load of 300 g for all tests. The indentation duration was 15 sec.

The density of manufactured samples is measured by image contrast method.

### 3. Results and discussion

#### 3.1. SLM procedure

It was shown by (Shishkovsky *et al.*, 2012) and by (Zaeh & Branner, 2010), the preheating of the substrate can significantly reduce the resulting cracking. The manufacturing chamber of the SLM machine was preheated up to  $600^\circ\text{C}$  during each experimentation as follows:

1. The cycle of protection gas filling launched at the same moment as the beginning of preheating ( $\text{O}_2 < 1000$  ppm reached after 30 min).
2. The complete building chamber was preheated, including the substrate and the powder, by the furnace integrated inside the SLM machine.
3. The SLM process started  $\sim 1,5\text{-}2$  h after the manufacturing chamber reached the temperature of  $600^\circ\text{C}$ .

Three different substrate materials are applied (SS 304L, Ti-6Al-4V, Inconel 718) in the following parameter windows: laser power ( $P$ ) 90-150 W, scanning speed ( $V$ ) 1400-3000 mm/s, scanning distance ( $S$ ) 70-110  $\mu\text{m}$ , powder bed thickness ( $h$ ) 30-50  $\mu\text{m}$ . Criss-cross strategy was applied (laser scan direction turned at  $90^\circ$  for odd layers). In several experiments, the rescanning of each layer was applied: in this case laser rescans previously remelted layer in the middle between solidified tracks.

Table 2. Thermal properties of the substrates and density of SLM samples

	Inconel 718	Ti-6Al-4V	Steel 304L	NiTi
Thermal conductivity, W/m K	11,4	7,2	16,2	18 – austenite 8,6 - martensite
CTE, $10^{-6} \times 1/^\circ\text{C}$	13,3	8,6	17,3	11 – austenite 6,6 – martensite
Max. Density of SLM sample, %	99,8	98,2	99,5	
Result	Longitude cracks	High porosity	Small amount of cracks + low porosity	

The relations between thermal properties of the substrates and resulting porosity is shown in Table 2. Optical images of the manufactured samples are shown in Fig. 2. Porosity was measured without taking into account the cracks. Inconel 718 substrate shows the best performance for the resulting density. However,

the elevated number of cracks was observed at cross-sections of the obtained samples. For further analysis, 304L steel substrate was chosen as it showed the optimal proportion between the number of resulting pores and cracks. Six specimens were manufactured with the following parameters:  $P=125$  W,  $V=2000$  mm/s,  $V_{rescan}=2250$  mm/s, criss-cross,  $h=30$   $\mu\text{m}$ ,  $S=80$   $\mu\text{m}$ .

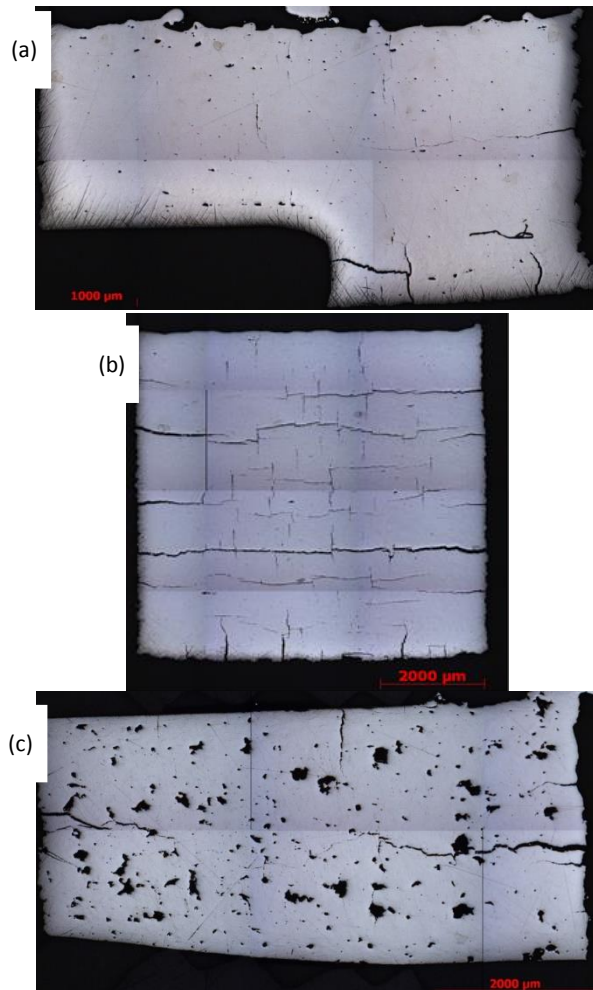


Fig. 2. SLM samples,  $P=125$  W,  $h=30$   $\mu\text{m}$ : (a) Inconel 718 substrate ( $P=125$  W,  $V=2000$  mm/s,  $V_{rescan}=2350$  mm/s,  $S=70$   $\mu\text{m}$ ); (b) Steel 304L substrate ( $P=125$  W,  $V=2750$  mm/s,  $V_{rescan}=2250$  mm/s,  $S=80$   $\mu\text{m}$ ) (c) Ti-6Al-4V substrate ( $P=125$  W,  $V=2200$  mm/s,  $S=100$   $\mu\text{m}$ )

### 3.2. Surface morphology

According to optical profilometer, the average roughness  $R_a$  of the top surface of the obtained samples is equal to  $9 \mu\text{m}$  and  $R_{\text{max}}$ , related to the formation of agglomerates during laser scanning, for all analyzed samples is in the range  $30\text{--}60 \mu\text{m}$  (Fig. 3a). For the lateral surfaces,  $R_a$  is  $14 \mu\text{m}$  and  $R_{\text{max}}$  is  $240 \mu\text{m}$ . The elevated value of the maximum roughness for lateral surfaces is caused by sticking of unmelted NiTi particles to these surfaces.

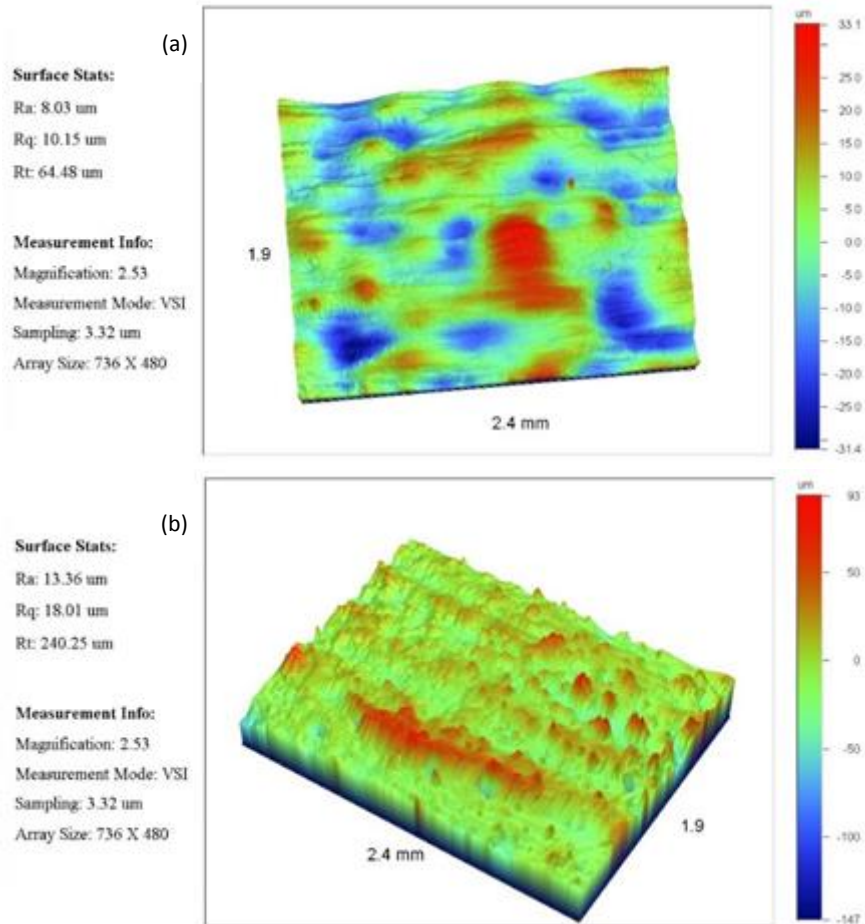


Fig. 3. Optical profilometer mapping for SLM samples (a) top surface (b) lateral surface

### 3.3. Microstructure and phase composition

XRD analysis shows that NiTi B2 austenite phase predominates in the initial powder, manufactured samples and non-melted powder heated up-to  $600^\circ\text{C}$  (Fig. 4). The monoclinic martensite B19' was found in

the initial and heat-treated powders. As it is shown in (Dadbakhsh *et al.*, 2016), this phase can be formed after SLM of NiTi without preheating. The narrow temperature hysteresis of the B2→R transformation determines a quite limited number of picks of the intermediate R phase. Heat treatment of the initial powder at 600°C during 3-5h does not result in dissolution of the cubic NiTi<sub>2</sub> phase. XRD shows that Ni<sub>4</sub>Ti<sub>3</sub> precipitates are formed after SLM of NiTi. (Adharapurapu, 2007) has shown that Ni<sub>4</sub>Ti<sub>3</sub> precipitates are formed after 0.5 h heat treatment of 60Ni-Ti alloy at 600°C; the small size of the formed precipitates does not allow distinguishing them by SEM.

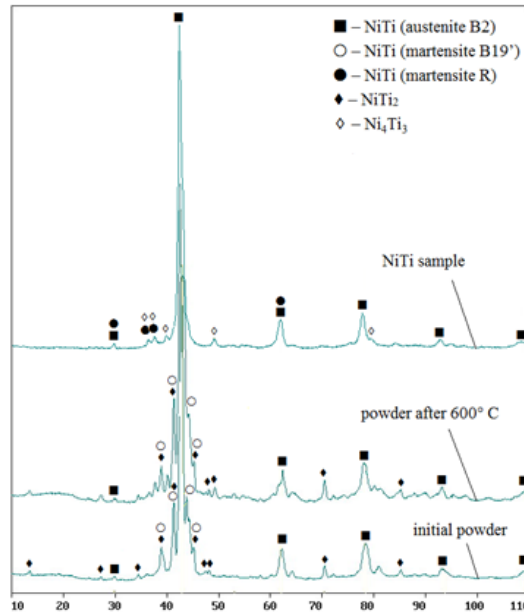


Fig. 4. XRD diffractograms of the initial powder, manufactured samples and heated up-to 600°C non-melted powder

To study the microstructure, the samples were etched by HCL+HNO<sub>3</sub>+HF reagent during 15 s. It was found that the resulting structure of the obtained samples is austenitic. Some zones of the incomplete martensitic transformation can be distinguished at the cross section (Fig. 5). No signs of Ni<sub>4</sub>Ti<sub>3</sub> precipitates were detected.

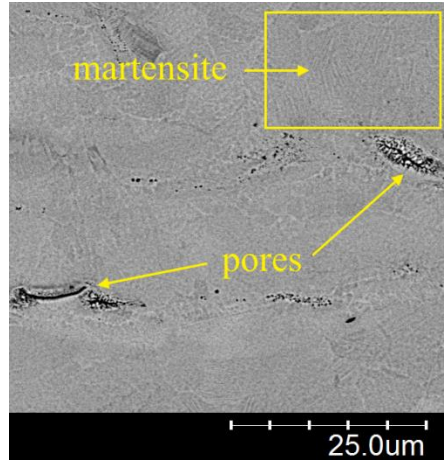


Fig. 5. Microstructure of the etched NiTi sample

### 3.4. Nanoindentation

To study mechanical behavior of the formed phases, the nanoindentation test was performed. Twenty-five nanoindentations were carried out with the step of 20  $\mu\text{m}$ . The majority of the points (about 80%) represents austenitic B2 phase. The presence of the intermediate R phase with lower Young's modulus was confirmed. The load-displacement curves are shown in Fig. 6.

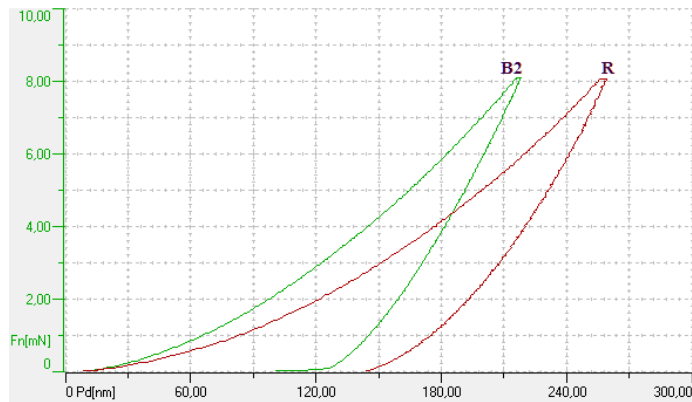


Fig. 6. Nanoindentation load-displacement curve of NiTi sample

The measured mechanical properties of the B2 and R phases are presented in Table 3.

Table 3. Mechanical properties of the B2 and R phases obtained by nanoindentation

Phase	Hardness, GPa	Young's modulus, GPa	Penetration depth, nm	Elastic recovery, %
B2	8,1	108	217	42,3
R	5,7	84,1	258	42,9

### 3.5. Cracking analysis

One can suppose that the brittle R phase represents the centers for relaxation of residual stresses. The martensite-like structure can be seen inside of the cracks (Fig. 7).

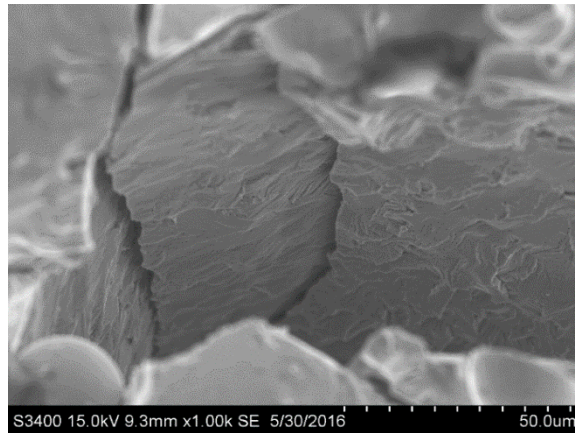


Fig. 7. Martensite-like structure inside of crack

Oxygen traces were detected by means of EDS in the manufactured samples and at the surface of the non-melted NiTi powder. The fraction of oxygen is 0,3-0,7% wt. at the polished cross-sections of the samples and it is 10-20% wt. at the surface of the heated up-to 600°C powder. This considerable difference probably is related to the elevated effective surface of oxygen absorption for the small size powder. It is known (Kofstad, 1967) that elevated temperature augments considerably the oxidation of pure titanium. (Zhu *et al.*, 2003) have shown that NiTi absorbs oxygen in the following way:  $\text{NiTi} + \text{O}_2 \rightarrow \text{Ni}_3\text{Ti} + \text{TiO}_2 \rightarrow \text{Ni}_4\text{Ti} + \text{TiO}_2 \rightarrow \text{Ni} + \text{TiO}_2$ , and the fraction of oxygen reaches 6,5% wt. at the depth of 80 nm after 30 min of heat treatment at 400°C for 30 min in ambient atmosphere of air.

One may conclude that the fraction of 0,1% wt. of oxygen inside of the manufacturing chamber is still quite critical for SLM of NiTi alloy with preheating up-to 600°C and results in oxidation of the powder.

## 4. Conclusions

- Influence of powder preheating: Powder preheating up-to 600°C allows reducing the thermal gradients during SLM of NiTi. At the same time, high-temperature oxidation of NiTi increases cracking of the



remelted powder. Cubic samples with the resulting oxygen fraction of 0.3-0.7% wt. were manufactured under the O<sub>2</sub> pressure less than 1000 ppm inside the manufacturing chamber.

- The substrate composition: It influences the resulting porosity and cracking of NiTi. On the one hand the lowest porosity, 0.2%, was obtained with Inconel 718 substrate; on the other hand using the steel 304L substrate allows obtaining the samples with practically the same density, 99.6%, but with considerably reduced number of cracks.
- Surface roughness: The elevated roughness at lateral surfaces of the manufactured samples ( $R_a=14\ \mu\text{m}$ ,  $R_{\text{max}}=240\ \mu\text{m}$ ) is caused by sticking of non-melted NiTi particles to these surfaces. The average roughness  $R_a$  at the top surface is equal to  $9\ \mu\text{m}$  and  $R_{\text{max}}=30-60\ \mu\text{m}$ .
- The main phase of the developed samples is NiTi B2 austenite. Some minor picks of R martensite were detected, as well as the formation of Ni<sub>4</sub>Ti<sub>3</sub> precipitates. Analysis of the non-melted powder after heat treatment at 600°C have shown no dissolution of NiTi<sub>2</sub> phase. The microstructure of the samples is composed from austenitic grains with martensitic zones of the R phase.
- Mechanical properties were measured by nanoindentation: Young's modulus of B2 austenite equals to 108 GPa and the hardness is equal to 8.1 GPa; for R martensite Young's modulus equals to 84.1 GPa and hardness is equal to 5.7 GPa.
- Martensitic structure was found inside the cracks; probably brittle R phase represents the centers for relaxation of residual stresses.

## Acknowledgment

The work was carried out with financial support from the Ministry of Education and Science of the Russian Federation in the framework of Increase Competitiveness Program of NUST «MISIS» (№ K1-2016-030), implemented by the governmental decree dated on 16th of March 2013, N 211.

## References

- Adharapurapu, R. R. (2007). Ph.D. thesis, UC San Diego.
- Dadbakhsh, S., Vrancken, B., Kruth, J.-P., Luyten, J. & Van Humbeeck, J. (2016). *Materials Science and Engineering: A* 650, 225-232.
- Kofstad, P. (1967). *Journal of the Less Common Metals* 12, 449-464.
- Sauthoff, G. (2008). *Intermetallics*. Weinheim, Germany: Wiley.
- Shishkovsky, I., Yadroitsev, I. & Smurov, I. (2012). *Physics Procedia* 39, 447-454.
- Yoneyama, T. & Miyazaki, S. (2008). *Shape memory alloys for biomedical applications*. Cambridge, England: Woodhead Publishing Limited.
- Zaeh, M. F. & Branner, G. (2010). *Production Engineering* 4, 35-45.
- Zhu, L., Trépanier, C., Pelton, A. & Fino, J. (2003). *Medical device materials*, edited by S. Shrivastava. Anaheim, Canada.